Journal of CO2 Utilization 67 (2023) 102340

Contents lists available at ScienceDirect

Journal of CO2 Utilization

journal homepage: www.elsevier.com/locate/jcou

An optofluidic planar microreactor with photoactive $Cu_2O/Mo_2C/TiO_2$ heterostructures for enhanced visible light-driven CO_2 conversion to methanol

Ivan Merino-Garcia [a,*], Gonzalo García [b], Ignacio Hernández [c], Jonathan Albo [a,*]

[a] Departamento de Ingenierías Química y Biomolecular, Universidad de Cantabria, Avenida de los Castros s/n, 39005 Santander, Cantabria, Spain
[b] Instituto de Materiales y Nanotecnología, Departamento de Química, Universidad de La Laguna, PO Box 456, 38200 La Laguna, Santa Cruz de Tenerife, Spain
[c] Departamento CITIMAC, Universidad de Cantabria, Avenida de los Castros s/n, 39005 Santander, Cantabria, Spain

ARTICLE INFO

Keywords:
Continuous CO_2 photoreduction
Optofluidic microreactor
Methanol
Visible light
$Cu_2O/Mo_2C/TiO_2$ heterostructures

ABSTRACT

Mixing TiO_2 with Mo_2C has recently been proposed to improve the photocatalytic conversion of CO_2 to methanol under visible light irradiation, although further efforts are still needed to enhance process performance. In this context, the use of *p-type* semiconductors (i.e., Cu_2O) in co-doping strategies can enhance not only the redistribution of electric charges due to its narrowing bandgap, but also the selectivity of the reaction towards methanol. This work focuses on the development of a continuous visible light-driven CO_2 photoconversion to methanol process in an optofluidic microreactor using $Cu_2O/Mo_2C/TiO_2$ heterostructures. A significant improvement in process performance can be seen under visible light with the heterostructures containing 4 wt% of Cu_2O. Superior methanol production rates (36.3 $\mu mol \bullet g^{-1} \bullet h^{-1}$) with an apparent quantum yield = 0.64% and a reaction selectivity = 0.93 are reached, in comparison with the results achieved at Cu_2O-free Mo_2C/TiO_2 photocatalytic surfaces (11.8 $\mu mol \bullet g^{-1} \bullet h^{-1}$, 0.21% and 0.92, respectively). This can be adscribed to the role of Cu_2O in the selectivity of the reaction towards methanol. The synergetic effect between Cu_2O, Mo_2C, and TiO_2 in the heterostructures may also provoke a more efficient charge separation and transfer, while enhancing the visible light absorption properties of the material and its photocatalytic stability. The maximum methanol rate outperforms most of the values previously reported in slurry batch reactors and evidences the possibility of enhancing the continuous visible light-driven CO_2-to-methanol photoconversion process with efficient metal co-doping approaches in optofluidic microreactors.

1. Introduction

CO_2 utilisation represents an interesting strategy for the generation of value-added products from sustabinable perspectives [1–3]. Among the different obtainable products, the production of alcohols such as methanol (CH_3OH) is widely studied owing to its importance in several applications, namely as a chemical storage carrier for hydrogen or as a platform product in gasoline and biodiesel [4–7]. Several CO_2 conversion approaches including thermochemical, biological, electrochemical, photoelectrochemical, and photochemical methods can be considered to meet the target [8,9]. For example, the electrochemical conversion of CO_2 to CH_3OH has been widely proposed to overcome the extreme operating conditions (temperature and pressure) of conventional thermocatalytic procedures, while storing excess of energy from renewable and intermittent green sources in the form of chemical bonds [10–12]. The photochemical approach using solar irradiation, by contrast, represents a more direct way of transforming CO_2 into CH_3OH at mild conditions without additional energy inputs, thus mimicking the natural photosynthesis process used by plants [13–15]. Therefore, this CO_2 conversion approach presents potential to close the carbon cycle while generating several value-added products simultaneously under the sun. Nevertheless, this technology still requires the development of cheap, active, efficient, stable, and environmentally-friendly photocatalysts for the activation of CO_2 molecule and its further light-driven transformation towards valuable chemicals [13,16,17].

Titanium dioxide (TiO_2) is the most applied semi-conductor so far in solar-fuel production strategies, and particularly for the generation of CH_3OH, due to its photo-stability, wide availability, and low-cost

* Corresponding authors.
E-mail addresses: merinoi@unican.es (I. Merino-Garcia), alboj@unican.es (J. Albo).

https://doi.org/10.1016/j.jcou.2022.102340
Received 18 February 2022; Received in revised form 27 September 2022; Accepted 21 November 2022
Available online 29 November 2022

properties, among others [18]. The photocatalytic activity and efficiency of TiO_2 under sunlight exposure is, however, limited by its wide bandgap (> 3 eV), which makes this material active mainly in the UV light region [19]. Regrettably, the sunlight spectrum is composed only of 4% UV light (< 380 nm) but ~44% of visible light (380–700 nm). Besides, TiO_2 also exhibits poor electron-hole pair separation (rapid recombination) and low adsorption capacity for CO_2, thus leading to additional photocatalytic efficiency limitations for CO_2 converison [20,21]. As a consequence, the research community is focused on the design and development of efficient procedures capable of enhancing the activity and performance of TiO_2 under visible light. In this respect, the use of Mo_2C-based photocatalysts under visible light has been reported before, either for hydrogen production [22,23] or CO_2 conversion [20,24]. These materials possess improved catalytic properties than alternative noble metals in terms of stability, selectivity, and opposition towards poisoning [24]. Thus, the potential benefits of incorporating metal carbides in CO_2 photoreduction to improve the performance of bare TiO_2 under visible light exposure are well-founded. In particular, mixing TiO_2 with synthesised Mo_2C nanoparticles was recently found to enhance the visible light-driven photocatalytic conversion of CO_2 into CH_3OH over bare TiO_2 (CH_3OH production rate: 11.8 vs. 0.11 $\mu mol \cdot g^{-1} \cdot h^{-1}$) as a function of the mass percentage of Mo_2C incorporated in the blends [20]. This finding was explained by an improved interfacial conductivity, an efficient separation of electron-hole pairs, as well as a decrease in the bandgap energy of the photocatalytic material compared to bare TiO_2. However, CH_3OH production rates, reaction selectivity, and photocatalytic efficiencies were still far from those values achieved under UV irradiation. Hence, additional metal co-doping strategies can be applied to enhance the performance of Mo_2C/TiO_2 blends, decreasing the bandgap energy of the material and increasing the presence of actives sites for CO_2 photoactivation and conversion. Previous reports show how copper (Cu)-derived catalysts (e.g., oxide-derived Cu) can be effective and selective for the conversion of CO_2 to CH_3OH in both electrochemical [4,7,25–27] and photochemical strategies [13,28–30]. In the latter approach, the combination of TiO_2 and Cu-derived materials involves favourable reaction mechanisms for the selective production of CH_3OH, thereby facilitating the overall photoreduction performance [13,31]. In particular, copper (I) oxide (Cu_2O) is a relatively abundant and cheap *p-type* semiconductor with specific optical and light absorption properties, a narrow bandgap energy (2–2.2 eV), and suitable conduction and valence band positions [32–36]. Thus, the incorporation of Cu_2O particles in heterostructures can reduce the recombination of photogenerated charges, improve their redistribution in the photocatalytic surface, and enhance the selectivity of the reaction towards methanol formation [13,31].

Last but not least, not only active, stable, and selective photocatalytic materials are required to move forward into the implementation of CO_2 photoreduction technologies, but also the development of efficient photoreactor configurations with improved surface-area-to-volume ratio to optimise the exposure of photocatalytic active sites to light irradiation and facilitate the photoconversion of CO_2 towards CH_3OH simultaneously [37–39]. In this respect, the use of optofluidic devices (as a synergy of microfluidics and optics) has been proposed to provide uniform light distribution, flow control, enhanced mass transfer, and large surface-area-to-volume ratios [13,40]. Among the available optofluidic microreactors, planar configurations seem to achieve superior performance in photocatalytic processes, owing to a larger photon receiving area [20,31,41].

Thus, in this work we propose the development of a planar optofluidic microreactor with improved characteristics compared to common slurry batch reactors, for enhanced continuous CO_2 photoreduction to CH_3OH using visible light active $Cu_2O/Mo_2C/TiO_2$ heterostructures. The results in the visible region are compared to those previously reached at Cu_2O-free Mo_2C (4 wt%)/TiO_2 blends in the same photoreactor configuration to demonstrate the potential applicability of the prepared samples, thereby providing novel insights into the development of efficient, stable, and selective systems for the continuous production of CH_3OH from CO_2 photoreduction.

2. Material and methods

2.1. Synthesis and characterisation of $Cu_2O/Mo_2C/TiO_2$ photocatalysts

The Mo_2C nanoparticles are synthesised by a slightly modified standard carbothermal method that has been described in detail elsewhere [20,42]. In brief, a molybdenum oxide precursor (MoO_3) is firstly dissolved in ammonium hydroxide (NH_4OH) solution under agitation at room temperature, namely "Sample 1". Subsequently, a suspension of carbon black in ethanol (CH_3CH_2OH) is prepared by sonication, namely "Sample 2". Then, "Sample 1" is added (drop by drop) into "Sample 2" at room temperature under stirring conditions. A dry powder is produced after increasing the temperature up to 60 ºC. Finally, the obtained dry powder is grounded in a mortar and afterwards introduced in a tube furnace under H_2/N_2 (5 v.%) atmosphere from room temperature to 800 ºC.

Thereafter, the nanometric synthesised Mo_2C particles are physically mixed with TiO_2 (P25 ≥ 99.5%, Sigma-Aldrich) to produce Mo_2C (4 wt %)/TiO_2 blends. This Mo_2C weight percent is selected for an enhanced CH_3OH production and reaction selectivity [20]. Finally, different amounts (2–10 wt%) of commercial Cu_2O particles (particle size < 5 μm, 97% purity, Sigma-Aldrich) are added to the synthesised Mo_2C/TiO_2 samples to obtain different Cu_2O/Mo_2C (4 wt%)/TiO_2 composites, as listed in Table 1.

Scanning electron microscopy (SEM, equipped with Energy Dispersive X-ray microanalysis (EDX, Oxford X-Max 50)) and high resolution transmission electron microscopy (HR-TEM) measurements are acquired using a Zeiss Evo 15 microscope and a Jeol JEM 2100 microscope, respectively, to evaluate the size, morphology, and elemental composition of the prepared photocatalysts. Besides, X-ray diffraction (XRD) spectra are measured by an X'Pert PRO X-ray diffractometer (PANaytical) to determine the crystal orientation of the photocatalytic structures. Thus, a CuKα radiation (λ = 1.5405 Å) is used in a range of 2 Theta data from 20 to 100 degrees (scan rate = 0.04 degrees·s^{-1}). The different crystalline phases are then identified by comparing the experimental response to the Joint Committee on Powder Diffraction Standards (JCPDS). Moreover, Raman patterns are acquired in a SPELEC RAMAN (Metrohm DropSens) apparatus with a green laser (λ = 532 nm) that operated in the 100–3200 cm^{-1} range. On the other hand, diffuse reflectance spectroscopy (DRS) analyses are carried out in a spectrophotometer (Agilent Technologies Cary 5000) to determine the diffuse reflectance in the UV–VIS–NIR region. Furthermore, N_2 adsorption–desorption isotherms are measured at − 196 °C using a Micromeritics ASAP 2020, and specific BET areas are calculated from the Brunauer, Emmett and Teller equation. Finally, an Edinburgh Instruments FLSP 920 double grating fluorometer equipped with a Xe lamp, Hamamatsu R928 and H10330C-75-C3 photomultiplier tubes allowed for photoluminescence (emission and excitation) analyses to study the optical properties of different photocatalytic samples (powder or deposited onto porous carbon paper) in both wet and dry conditions. Spectra are corrected for intensity factors.

Table 1
Composition and nomenclature of the prepared photocatalysts.

Photocatalytic material	Cu_2O content (wt%)	Nomenclature
Cu_2O-free Mo_2C (4 wt%)/TiO_2	0	Mo_2C4
Cu_2O/Mo_2C (4 wt%)/TiO_2	2	$Cu2Mo_2C4$
	4	$Cu4Mo_2C4$
	6	$Cu6Mo_2C4$
	8	$Cu8Mo_2C4$
	10	$Cu10Mo_2C4$

2.2. Manufacturing of photoactive surfaces

The photoactive light-responsive surfaces are prepared by following an airbrushing procedure. In a first step, a photocatalytic ink containing the heterostructures is prepared using a Nafion® dispersion (5 wt%, Alfa Aesar) as a binder, and isopropanol (IPA, Sigma-Aldrich) as a vehicle, with a 70/30 (photocatalyst/Nafion) mass ratio and a 3 wt% of total solids (photocatalyst + Nafion). Secondly, after sonication, the resulting ink is airbrushed onto a porous carbon paper (TGP-H60, Toray Inc.) support covered by a paper mask with a hole of 1 cm^2. This Toray paper support is selected due to its notable gas transfer properties, thus facilitating the transport of CO_2 and diffusion of products [7]. Nafion may enhance the local proton activity in the vicinity of the photocatalyst surface, promoting proton-coupled multielectron transfer reactions, stabilizing intermediates, and inhibiting the re-oxidation of CO_2 reduction products [43]. The airbrushing process is carried out at 100 ºC to ensure the complete evaporation of IPA during the accumulation of photocatalytic layers. In this study, a photocatalytic loading (L) of 2 $mg{\cdot}cm^{-2}$ (experimentally determined by weighing) is selected based on previous findings [13]. The light-responsive surfaces are then dried at ambient pressure and temperature for 24 h and rinsed with deionised water before use. It can be confirmed based on a previous report [4,13] that the photocatalyst is well bonded to the substrate after the airbrushing process, since the weight loss of the photoactive surface was less than 10% after 4 h of continuous visible-light driven CO_2 photoreduction to methanol in the same optofluidic microreactor.

2.3. Performance of $Cu_2O/Mo_2C/TiO_2$ heterostructures in an optofluidic microreactor

A home-made designed planar optofluidic microreactor (APRIA Systems S.L.) with a reaction microchamber of 1 cm^2 and 75 μL is applied to evaluate the performance of the prepared heterostructures in continuous mode under ambient conditions. A detailed representation of both the micro-optofluidic photoreactor characteristics and the lab-scale experimental setup can be found in the supporting information. Briefly, the light-responsive surfaces are sandwiched between two highly transparent polymethylmethacrylate (PMMA, Altuglas-Arkema) plates and a stainless-steel plate on the top. The photocatalytic material is located in the centre of the reaction chamber of the PMMA plate, and irradiated with visible (450 nm) or 1200 mW UV (365 nm) LED lights with a light intensity of E = 5 $mW{\cdot}cm^{-2}$, measured by a radiometer (Photoradiometer Delta OHM). The experiments are carried out in continuous mode for 120 min, even though the stability of the photocatalysts has also been evaluated in the long-term (7 h). An infrared thermometer controls the temperature during the operation. A CO_2-saturated 0.5 M $KHCO_3$ (Panreac >97%) aqueous solution is pumped (peristaltic pump, Miniplus 3 Gilson) to the liquid microchamber at a flow rate of 50 $\mu L{\cdot}min^{-1}$. A collection vessel is placed at the microreactor outlet to collect samples every 30 min, which are finally analysed (by duplicate) in a headspace gas chromatograph (GCMS-QP2010 Ultra Shimadzu) equipped with a flame ionization detector (FID). Besides, the concentration of $HCOO^-$ is measured with Ion Chromatography (Dionex ICS 1100).

The performance of the continuous CO_2 photoreduction process is evaluated by: i) production rate (r, in $\mu mol{\cdot}g^{-1}{\cdot}h^{-1}$), defined as the concentration of product per gram of photocatalyst and time; ii) selectivity (S), which corresponds to the ratio between the production rate for CH_3OH and the cumulative product rates (r for CH_3OH + r for $HCOO^-$); and iv) apparent quantum yield (AQY), defined in Eq. (1) as follows:

$$AQY(\%) = \frac{n_e}{n_p} \times 100 \quad (1)$$

where n_e represents the rate of electrons transferred towards CH_3OH, defined as the number of molecules evolved (mol) multiplied by the number of reacted electrons (6 e^- for CH_3OH) and the Avogadro's number (mol^{-1}). On the contrary, n_p is the rate of incident photons on the surface, calculated according to the following equation:

$$n_p = \frac{E{\cdot}A{\cdot}t{\cdot}\lambda}{h{\cdot}C} \quad (2)$$

where E is the light intensity ($W{\cdot}m^{-2}$), A represents the irradiation area (m^2), t is the reaction time (s), λ corresponds to the wavelength peak (m), h is the Planck's constant (J·s) and C represents the speed of light ($m{\cdot}s^{-1}$), respectively.

3. Results and discussion

3.1. Characterisation of $Cu_2O/Mo_2C/TiO_2$ photocatalysts

Fig. 1 shows the SEM images of individual catalysts (Fig. 1a and Fig. 1b: spherical Mo_2C and Cu_2O particles, respectively) and several $Cu_2O/Mo_2C/TiO_2$ photocatalytic samples, namely Cu2Mo_2C4 and Cu4Mo_2C4 (Fig. 1c and Fig. 1d, respectively). The particle size of the bipyramid Cu_2O (< 5 μm) [7] and pseudospherical TiO_2-P25 (21 nm) particles [44,45] is given by the commercial manufacturer of the materials (Sigma-Aldrich). Besides, the average particle size of the synthesised Mo_2C particles was determined to be < 20 nm in a previous study [46], where additional details about their pseudospherical morphology, crystalline phases, binding energy, and their electrochemical activity can be found. The structure and morphology of Mo_2C/TiO_2 blends have also been described in detail in a previous report [20]. In the present study, the different selected SEM images of Cu2Mo_2C4 and Cu4Mo_2C4 (please see all SEM images in the supporting information), reveal in Fig. 1c and Fig. 1d, respectively, that the distribution of the photocatalysts is homogeneous after the physical incorporation of Cu_2O into Mo_2C (4 wt%)/TiO_2 blends, in agreement with the results achieved in previous reports of our group for Mo_2C/TiO_2 and Cu/TiO_2-based surfaces prepared by the same airbrushing method [13,20]. Additionally, Fig. 2 shows the HR-TEM images for Cu4Mo_2C4 and Cu10Mo_2C4 heterostructures, where apart from a homogeneous distribution, an efficient connection between the three components can be seen. The use of ternary composites may provoke an effective interfacial charge transfer among Cu_2O, Mo_2C, and TiO_2 for an enhanced

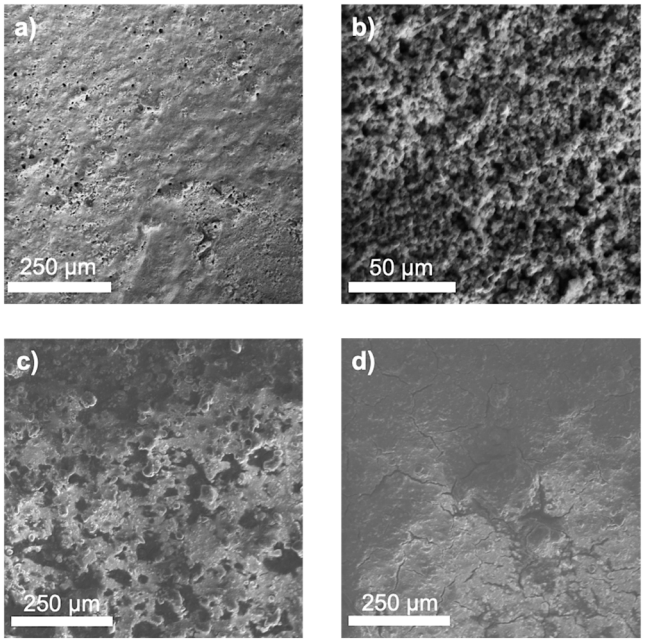

Fig. 1. SEM images for: a) Mo_2C, b) Cu_2O, c) Cu2Mo_2C4, and d) Cu4Mo_2C4 composites.

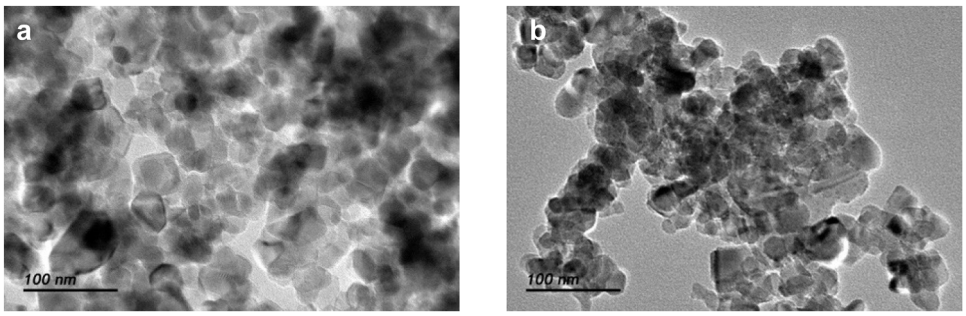

Fig. 2. HR-TEM images for: a) $Cu4Mo_2C4$ and b) $Cu10Mo_2C4$.

photocatalytic activity [47].

Fig. 3 displays, as an example, the corresponding elemental mapping of $Cu4Mo_2C4$. The colour sorting used clearly shows the existence of Cu, O and C elements, together with Ti and Mo, which evidences the successful synthesis of $Cu_2O/Mo_2C/TiO_2$ composites. Further details about the elemental composition of the different prepared photocatalytic materials can be found in the supporting information.

Moreover, Table 2 shows the specific BET area values of the heterostructures compared to Mo_2C4 (Cu_2O-free), pure Cu_2O, and pure Mo_2C particles. The averaged surface area of TiO_2 nanoparticles is determined by the commercial manufacturer (50 $m^2 \cdot g^{-1}$). The heterostructures present surface areas ranging from 45.5 to 55.2 $m^2 \cdot g^{-1}$, which are significantly higher than those values (experimentally measured) for Cu_2O (1.8 $m^2 \cdot g^{-1}$), Mo_2C (0.7 $m^2 \cdot g^{-1}$), and Mo_2C4 particles (30.1 $m^2 \cdot g^{-1}$). As expected, $Cu_2O/Mo_2C/TiO_2$ surface areas are similar to that of TiO_2, since it is the predominant component in the heterostructures. Larger photocatalytic surface areas might lead to an increased number of available actives sites for receiving photon and electron-hole pairs formation.

Fig. 4 exhibits XRD patterns for different prepared heterostructures as a function of Cu_2O content. With respect to TiO_2 presence, both rutile and anatase crystalline phases are identified in the five prepared photocatalysts. These specific TiO_2 phases have been previously reported to be essential for reaching maximal photocatalytic activity and performance in TiO_2-based materials [48,49]. The corresponding diffraction peaks of anatase (JCPDS card no. 21–1272) as a function of 2 Theta (from lower to higher degrees) can be seen in Fig. 3, namely (101), (103), (004), (112), (200), (105), (211), (204), (116), (220), and (215) crystal facets, respectively. TiO_2 rutile (JCPDS card no. 21–1276) displays, on the other hand, the following crystal planes: (110), (101), (111), (211), (220), (200), (301), and (112), as 2 Theta increases.

Table 2
BET specific surface area of Cu_2O, Mo_2C and different $Cu_2O/Mo_2C/TiO_2$ heterostructures.

(Photo)catalyst	BET surface area ($m^2 \cdot g^{-1}$)
Cu_2O	1.8
Mo_2C	0.7
Mo_2C4	30.1
$Cu2Mo_2C4$	47.0
$Cu4Mo_2C4$	55.2
$Cu6Mo_2C4$	48.3
$Cu8Mo_2C4$	52.1
$Cu10Mo_2C4$	45.5

Besides, the visible Mo_2C diffraction peaks (please see yellow spectra) reveal (100), (002), (101), (102), (110), (103), (112), and (201) crystal orientations according to JCPDS card no. 01–1188. It should be noted that the response for Mo_2C is clearly lower than that for TiO_2 (predominant in the heterostructures), in agreement with a previous study at Mo_2C/TiO_2 blends [20]. The diffraction patterns that correspond to Mo_2C can be seen in detail in a previous report [46]. Finally, the presence of Cu_2O is demonstrated by comparing the obtained spectra with JCPDS card no. 05–0667 reference. In this respect, (110), (111), (200), (211), (220), (311), and (222) crystal orientations can be clearly observed. It is important to highlight here that several specific diffraction peaks become more visible as the content of Cu_2O increases in the heterostructures, such as (111), (200), and (220) facets, observed at 2 Theta = 36.4°, 42.3° and 61.4°, respectively. Thus, these three specific crystal planes are predominant in the prepared photoactive heterostructures. Among them, the Cu_2O (111) structure has recently exhibited superior stability and selectivity towards alcohol production from CO_2

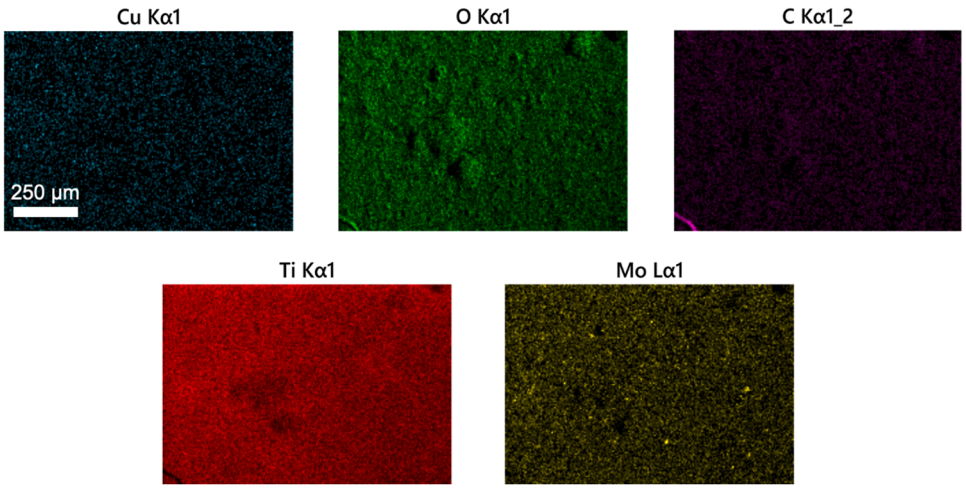

Fig. 3. Elemental mapping of $Cu4Mo_2C4$.

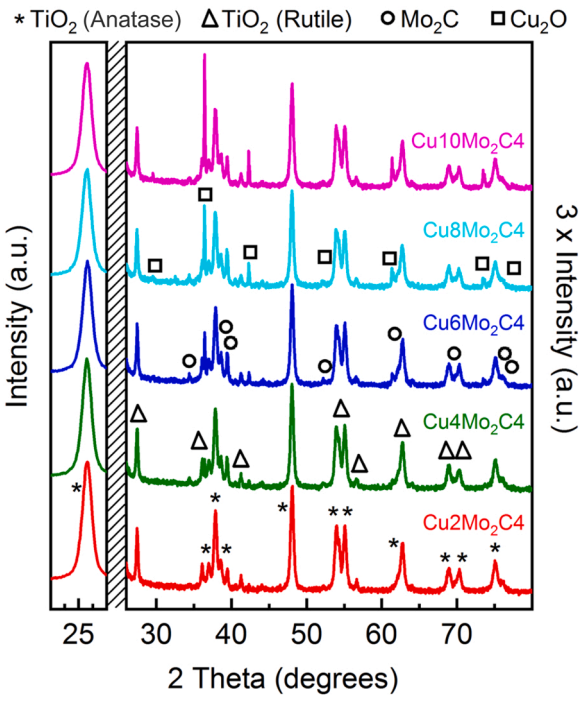

Fig. 4. XRD patterns of different Cu_2O/Mo_2C (4 wt%)/TiO_2 samples.

conversion in comparison with (200) and (220) crystal planes, due to the promotion of electron migration and the presence of oxygen-vacancy defects that facilitate CO_2 activation [50].

On the other hand, the Debye–Scherrer equation is used to estimate the crystallite size of Mo_2C and TiO_2. Average metal crystallite sizes of 20.35 nm and 30.79 nm are calculated from the largest peaks at 25.2° (TiO_2: anatase phase) and at 34.3° (Mo_2C), respectively. Due to the nanometric size of Mo_2C and TiO_2, similar particle size values are obtained from the diffractogram analysis in comparison with SEM measurements and previous TEM findings. However, this approach is not applicable to Cu_2O powder, since the Debye–Scherrer equation relates the crystallite size of sub-micrometer partices and it cannot be therefore considered to powders larger than 0.1 μm [46].

The Raman spectra of Cu_2O (black line) and $Cu_2O/Mo_2C/TiO_2$ composites are depicted in Fig. 5 (left). Firstly, the response of Cu_2O reveals a very low intensity signal since it is important to note that the intensity is increased by ten in the figure. In this respect, Raman peaks at 151.5 $\Gamma_{15}^{(1)}(LO)$, 207.5 $\Gamma_{12}^{-}$and 623 $\Gamma_{15}^{-(2)}$cm^{-1} can be discerned [51]. As was described in a previous report, Raman spectra of Mo_2C are not visible at the prepared $Cu_2O/Mo_2C/TiO_2$ samples due to the small size (shell) of molymbdenun oxide species (2–3 nm) presented in the Mo_2C (core), which seem to be below the detection limit of the Raman instrument [20]. On the other hand, Raman peaks associated to the anatase phase of TiO_2 are facile observed at 140 cm^{-1}: E_g; 191 cm^{-1}: E_g; 390.5 cm^{-1}: $B_{1\,g}$; 513.5 cm^{-1}: ($B_{1\,g}$ + $A_{1\,g}$); and 631.5 cm^{-1}: E_g. The peak at 441 cm^{-1} represents the weakest one and it is associated with the E_g mode of the rutile phase of TiO_2 [20], as observed in XRD analyses (Fig. 4). Overall, the whole Raman intensity decreases with the Cu_2O content in the photocatalytic samples.

Besides, most of Raman signals reveal insignificant variations in their relative intensities, full width at half maximum (FWHM), areas and positions. However, two of the signals (i.e., 513.5 and 631.5 cm^{-1}) develop Raman shift as a function of Cu_2O content in the composites (please see right panel of Fig. 5). A zoomed part of the shifted peaks is included in the supporting information for the sake of clarity. This finding can be explained by changes in the sample composition, defects and interactions caused by Cu_2O content, specially at high Cu_2O loadings (particle agglomeration), as previously observed in BET measurements (decreased surface area as the content of Cu_2O increases) and SEM images. This is in accordance with previous literature, where the lower performances of (photo)catalytic surfaces at high loadings during CO_2 conversion have been widely related to particle agglomeration [7,13,52–54]. The position of the signal at 631.5 cm^{-1} is similar for $Cu2Mo_2C4$ and $Cu4Mo_2C4$ samples but shifts towards lower wavenumbers when the content of Cu_2O in the heterostructures increases, which denotes that this signal represents a convolution between TiO_2 and Cu_2O signals, due to the opaque characteristics of Cu_2O [55]. Thus,

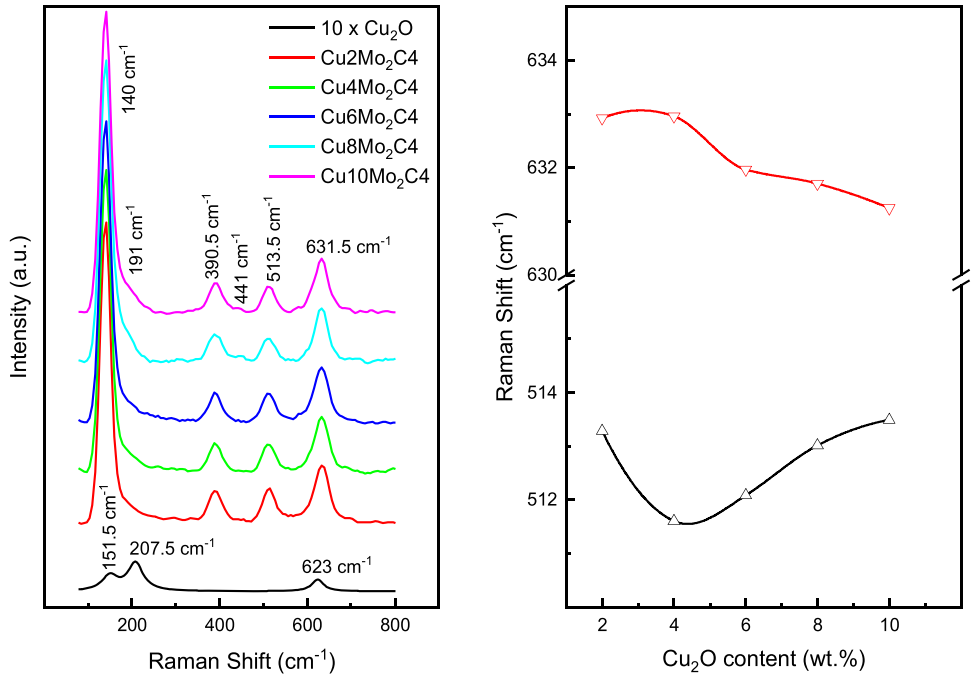

Fig. 5. Raman spectra of $Cu_2O/Mo_2C/TiO_2$ composites in comparison with Cu_2O (left panel) and shift in the E_g (red line) and $B_{1\,g}$ + $A_{1\,g}$ (black line) band position with Cu_2O content (right panel).

this Raman analysis might indicate an effective formation of Cu_2O/-Mo_2C/TiO_2 heterostructures for $Cu4Mo_2C4$, as a promising well-bonded photocatalytic material for CO_2 photoconversion to CH_3OH. On the other hand, the signal at 513.5 cm^{-1} reveals a strong Raman shift towards lower wavenumbers from $Cu2Mo_2C4$ to $Cu4Mo_2C4$, and then the signal shifts towards positive wavenumber at higher Cu_2O loadings. The Raman shifts for both signals at Cu_2O contents higher than 4 wt% (specular signals) can be initially related with the Raman signal of Cu_2O at 623 cm^{-1}, which increases with Cu_2O loading and disturbs the response of anatase signals, as demonstrated in XRD characterisation (Fig. 4). However, the strong red shift developed by the $Cu4Mo_2C4$ sample can be ascribed to a tensile strain of both vibrational modes ($B_{1\,g}$ + $A_{1\,g}$) caused by the effect of Cu_2O content in the heterostructures.

The UV-Visible absorption analyses displayed in Fig. 6a show the absorbance response of the photocatalysts in both visible and UV regions. A higher magnification analysis (Fig. 6b) has been made in order to compare the responses in the visible region as a function of Cu_2O content. As observed, the absorption can be enhanced in the visible spectra as increases the amount of Cu_2O in the samples up to 8 wt%, which can be explained by the presence of Cu_2O (a *p-type* semiconductor active under visible-light) [47,56,57]. Further increases in Cu_2O content (10 wt%) involved a reduction in absorption, as can be observed by comparing the visible spectra of $Cu8Mo_2C4$ (blue line) and $Cu10Mo_2C4$ (black line) samples. This tendency might be explained by increased shadow effects and particle agglomeration at higher amounts of Cu_2O, as confirmed by BET results (Table 2) and Raman spectra (Fig. 5), as well as by an enlarged material thickness that involves the formation of undesirable boundary layers.

Moreover, the estimated optical bandgap energies of the synthesised photocatalytic samples are calculated using the Kubelka-Munk method; in other words, the $[F(\text{reflectance}, R)\cdot h\nu]^2$ vs. photon energy ($h\nu$) plot is depicted, as can be seen in Fig. 7. The optical bandgap energies of the photoactive Cu_2O/Mo_2C/TiO_2 heterostructures (ranging from 3.08 to 3.15 eV) are lower than those results achieved for Cu_2O-free Mo_2C/TiO_2 blends (3.22–3.36 eV) and bare TiO_2 (3.48 eV) [20], which can be initially assigned to the presence of Cu_2O (narrow bandgap of 2.03 eV) [58–60] in the photoactive heterostructures. This is in agreement with previous literature [61], which shows that the addition of Mo_2C in heterostructures leads to a decrease in their bandgap with respect to the bandgap value of the main component (P25 in this case). Decreasing the optical bandgap energy of the photocatalyst should lead to an improved process performance since the narrowing in the bandgap would favour the absorption of solar energy in the visible region and the excitation of electrons from the valence band to the conduction band simultaneously [34]. Although an ideal photocatalyst should function in the visible region with an optical bandgap of less than 3 eV [62], the literature shows how the use of heterostructures with an optical bandgap near 3 eV can be highly active under visible light [63–65]. In this regard, the

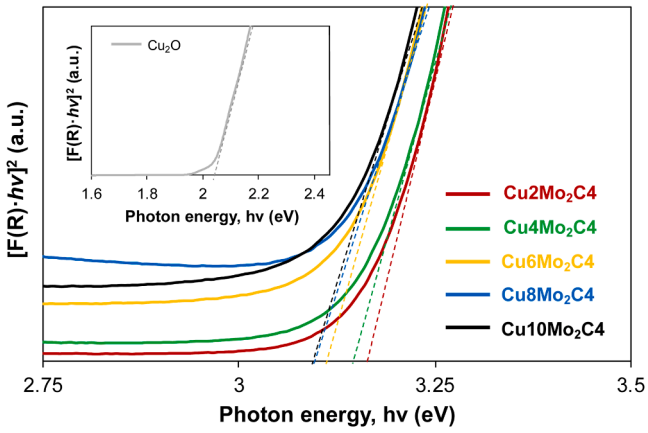

Fig. 7. Bandgap energy plot (Kubelka-Munk function) of Cu_2O/Mo_2C/TiO_2 samples and Cu_2O particles.

proposed heterojunctions display comparable bandgap values with respect to previous visible light-active photocatalysts reported.

With respect to the optical properties, Cu_2O shows an almost negligible photoluminescence (please see the supporting information) upon UV or visible excitation, in agreement with previous studies for such a pure copper compound at ambient temperature [66]. TiO_2-P25 also displays a very reduced intragap luminescence upon valence band excitation (please see the supporting information) according to the literature, caused by blue-emitting traps [67,68]. As a result, the photoluminescence discussion is therefore focused on the optical properties of Mo_2C.

While Cu_2O is not luminescent at the excitation wavelengths, photoluminescence spectra of the Mo_2C powder (dry conditions) show the occurrence of an emission/excitation in the energy region comprised within the TiO_2 gap (Fig. 8). The 430 nm photoluminescence and 355 nm excitation peaks (the latter corresponding to a pseudo-gap in the bulk Mo_2C band structure [69,70]) do appear closely to the UV and visible wavelengths used in the continuous photocatalytic conversion of CO_2 to CH_3OH. The occurrence of states in this energy range implies that the electronic structure of Mo_2C particles synthesized by a carbothermal method yields beneficial optical properties to be applied in light-driven CO_2 conversion approaches, especially under visible light irradiation. This excitation and luminescence can also contribute in harvesting the visible/near UV range, as it occurs mostly below the TiO_2 bandgap.

Moreover, the Mo_2C nanoparticles' absorption spectrum in the visible region is also studied under an aqueous environment in Mo_2C powder and Mo_2C films (2 $mg\cdot cm^{-2}$) supported onto toray carbon paper (please see the supporting information). Interestingly, we observe a decreased relative reflectivity of the wet samples in the visible spectrum.

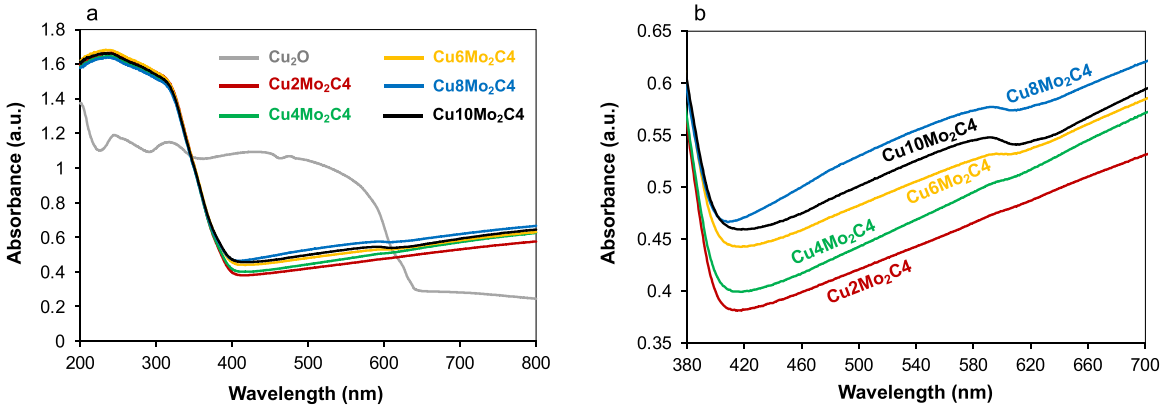

Fig. 6. a) UV-Visible absorption spectra of the heterostructures compared to Cu_2O; b) higher magnification of composite absorption responses in the visible region.

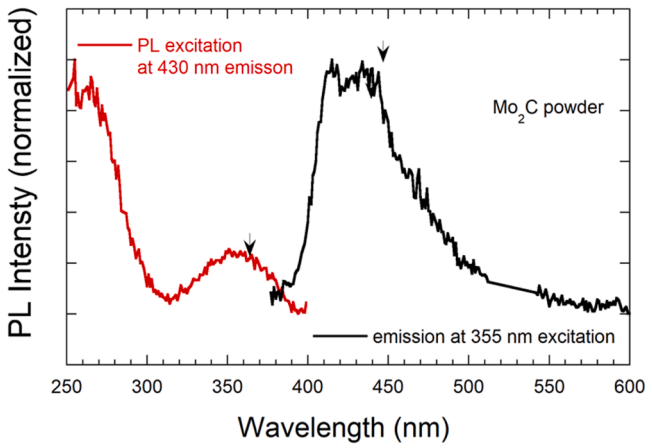

Fig. 8. Photoluminiscence (excitation and emmision) spectra of pure Mo_2C powder. The emission spectrum is taken at the corresponding 355 nm excitation wavelength and the photoexcitation spectrum is taken at 430 nm emission. The black arrows indicate the wavelengths employed for the CO_2 photoreduction experiments (365 nm: UV; 450 nm: visible light irradiation).

Increased optical absorption in the low energy range reflects either polarization or doping effects on the semimetal nanoparticles in water [71,72]. Enhanced photoexcitation and mobility of carriers favor the photocatalytic activity of the heterostructure.

3.2. *Continuous light-driven CO_2 photoconversion in an optofluidic microreactor*

The use of $Cu_2O/Mo_2C/TiO_2$ photoactive surfaces in the presence of CO_2 led to the formation of CH_3OH (main product) and $HCOO^-$ (smaller quantities). The production of CH_3OH is expected, taken into consideration previous findings on the use of Cu_2O [4,73–75], Mo_2C/TiO_2 [20], and Cu/TiO_2 [13,76] materials in both electrocatalytic and photocatalytic CO_2 reduction approaches. Moreover, $HCOO^-$ can be an intermediate in the CO_2 conversion pathway towards CH_3OH, as also demonstrated before [5,77]. The formation of ethanol is not observed in any experiment, which can be related to the presence of Cu_2O (111) structure (selective for CH_3OH formation [50]) in the photocatalysts, as shown by XRD results (Fig. 4). Only traces of CO and CH_4 (AQY < 0.05%) as gas-phase reduction products are observed, in accordance with previous results using the same optofluidic microreactor and Cu/TiO_2 [13] and Mo_2C/TiO_2 [20] photoactive surfaces under visible light illumination.

Fig. 9 displays the performance of the prepared photoactive surfaces after 120 min of continuous operation under visible (a) and UV light (b) illumination. The results reached in a previous study at Cu_2O-free Mo_2C (4 wt%)/TiO_2 blends are also included for comparison (same operating conditions and experimental setup) [20]. It is worth mentioning that the production of CH_3OH per gram of photocatalyst and time can be remarkably improved when incorporating Cu_2O in the heterostructures. In fact, superior *r* for CH_3OH are achieved for the five different prepared photoactive surfaces under visible light irradiation, in comparison with the performance of Cu_2O-free Mo_2C/TiO_2 blends (see Fig. 9a). This does demonstrate the positive synergetic-induced properties of the photocatalytic structures investigated, where improved visible light absorption properties (Fig. 6 and Fig. 7), photoexcitation de-localization (Fig. 8), and decreased recombination rates of photogenerated charges may provoke an enhanced CO_2 photoreduction selectivity towards CH_3OH. The results also show that yields for CH_3OH can be tuned by controlling the amount of Cu_2O in the photoactive heterostructures. All in all, a maximum visible light-driven CH_3OH production (together with an enhanced *AQY*) is achieved at $Cu4Mo_2C4$ (4 wt% of Cu_2O), which represents a three-fold superior value than that reached at Cu_2O-free Mo_2C/TiO_2 under the same conditions ($r = 36.3$ vs. 11.8 $\mu mol \cdot g^{-1} \cdot h^{-1}$; $AQY = 0.64$ vs. 0.21%). The main explanations for this enhanced performance are an improved specific surface area of Cu-based sites in this photoactive heterostructure (Table 2), as well as improved optical and light absorption properties (Fig. 6, Fig. 7 and Fig. 8). Additionally, the presence of Cu_2O and Mo_2C in the photocatalysts may boost the visible light activity compared to that of bare TiO_2, which was unable to produce CH_3OH from CO_2 photoreduction under visible light illumination [13], due to a narrow optical bandgap energy of the $Cu_2O/Mo_2C/TiO_2$ materials, thus favouring the absorption of solar energy in the visible region and the excitation of electrons from the valence band to the conduction band simultaneously [34]. The superior photocatalytic performance of the prepared heterostructures might be attributed to a better separation and transfer of photogenerated charge carriers. The use of $Cu_2O/Mo_2C/TiO_2$ heterostructures may allow an improved separation rate of electron-hole pairs for an enhanced photoefficiency towards CH_3OH generation due to the favourable electronic band structure. Based on previous comprehensive mechanistic studies reported in the literature [78–80] it can be hypothesised that, at the operating wavelengths, conduction band (CB)-electrons of Cu_2O can be firstly injected into the CB of TiO_2 active sites, which is possible since the CB of Cu_2O is higher than the CB of TiO_2-P25 (CB potentials of −1.1 V vs. NHE [78] and −0.36 V vs. NHE [79], respectively). Then, the excited electrons in TiO_2 can be transferred to the active surface of Mo_2C, whose CB is lower than that of TiO_2 (CB $Mo_2C = -0.3$ V vs. NHE [79]) while holes in Mo_2C band structure may migrate to the VB of Cu_2O.

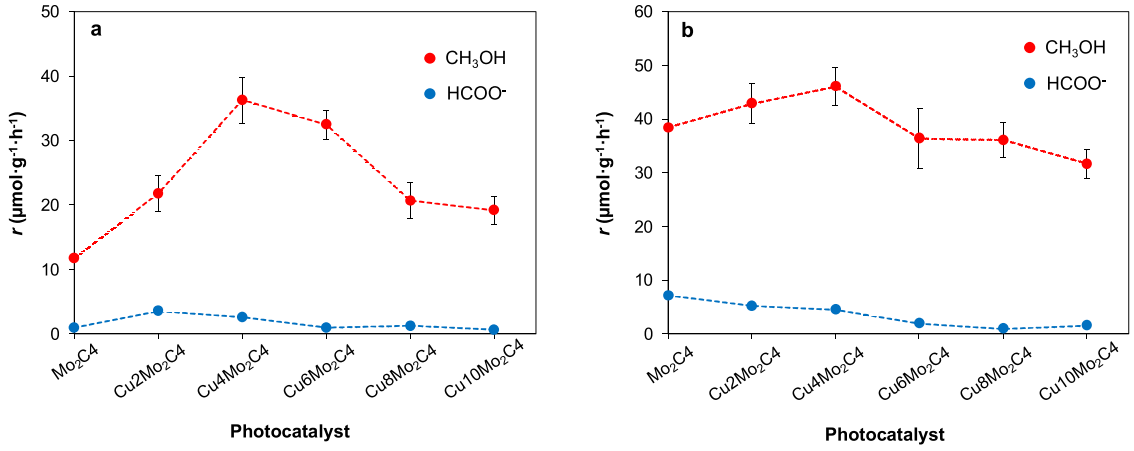

Fig. 9. Yields for methanol (CH_3OH) and formate ($HCOO^-$) in the continuous photoconversion of CO_2 at different $Cu_2O/Mo_2C/TiO_2$ heterostructures under a) visible and b) UV light irradiation.

Unfortunately, further increases in Cu_2O content (from 6 to 10 wt%) hinder the production of CH_3OH, which can be associated with shielding effects together with reduced specific BET surface area and particle agglomeration (Raman analyses) that lead to reduced photocatalytic activity. The synergetic effects between Cu_2O, Mo_2C, and TiO_2 in the visible spectrum also led to improved *AQY* for CH_3OH (please see the supporting information). This enhanced behavior is in accordance with the photoluminiscence analyses of Mo_2C, which leads to an improved electron-hole extraction and photocatalytic activity of the prepared heterostructures that favours the generation of CH_3OH from visible light-driven CO_2 conversion. The same tendency can be observed under UV light illumination (Fig. 9b), but with less remarkable changes with Cu_2O content.

In accordance with Fig. 9, the results displayed in Fig. 10 confirm the strong effect of Cu_2O content on reaction selectivity (*S*) to produce CH_3OH over $HCOO^-$ at the different heterostructures manufactured. As can be seen, Cu_2O contents higher than 2 wt% seems to be beneficial for selective CH_3OH generation from CO_2 photoconversion under both, visible and UV light illumination, with values of *S* ranging from 0.91 to 0.97. However, *S* appear to be hindered at a Cu_2O content of 2 wt%, especially under visible light conditions, which can be mainly associated with a lower visible light absorption (Fig. 6), an increased optical bandgap energy (Fig. 7), and specific reactive sites that lead to an enhanced $HCOO^-$ formation at Cu2Mo_2C4 (Fig. 9a). In any case, the production rate for CH_3OH using this heterostructure is clearly superior with respect to that reached with the Cu_2O-free surface under visible light irradiation (Fig. 9a), which highlights that the amount of Cu_2O active sites in the photocatalytic surface has a crucial role on the selectivity of the reaction (and so on reaction mechanisms) towards CH_3OH formation from CO_2 conversion, in agreement with previous studies [4,7,33,34,81–83]. Thus, dedicated and comprehensive mechanistic studies are required to provide further insights into the development of more efficient photocatalysts under visible light irradiation.

Overall, the best performance under visible light illumination for the continuous production of CH_3OH can be reached at a Cu_2O content of 4 wt%, namely Cu4Mo_2C4 photocatalyst ($r = 36.3$ μmol·g^{-1}·h^{-1}; *AQY* = 0.64%; $S = 0.93$). Finally, Fig. 11 compares the optimum *r* for CH_3OH (μmol·g^{-1}·h^{-1}) obtained in the present work with those values reached in different visible light-driven CO_2-to-CH_3OH studies using aqueous solutions in the last years [13,20,81,84–102], although different photocatalytic materials, electrolytes, experimental conditions, and photoreactor design/configurations are applied (please see Table S3 in the supporting information) [36]. Besides, superior CH_3OH rates have been reported elsewhere, but applying higher light irradiation intensities (i.e., 1200 W·m^{-2}) [76] or non-environmentally friendly organic solvents such as dimethylformamide, triethylamine, acetonitrile, and triethanolamine [36,103–116] that are able to facilitate the formation of CH_2 in the reaction mechanism towards CH_3OH generation from CO_2 conversion, although most of them are considered harmful and hazardous to human health.

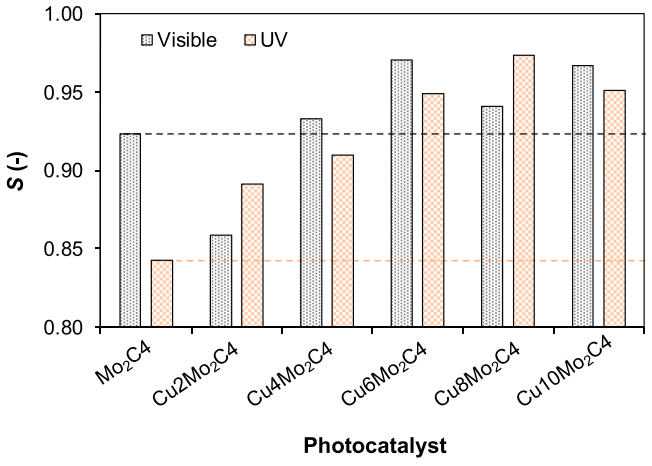

Fig. 10. Effect of Cu_2O content on reaction selectivity for CH_3OH in the photoactive surfaces under visible light (grey) and UV (orange) irradiation.

Interestingly, the maximum CH_3OH production rate reached at the $Cu_2O/Mo_2C/TiO_2$ heterostructures developed in the present study under visible light irradiation (red dot in Fig. 11: 36.3 μmol·g^{-1}·h^{-1}) is comparable and mostly superior to those values achieved from visible light-driven CO_2-to-CH_3OH photoreduction systems in aqueous solution. In particular, the results are more than three-fold improved in comparison with those observed at Cu_2O-free Mo_2C/TiO_2 blends [20] (green dot in Fig. 11: 11.8 μmol·g^{-1}·h^{-1}) under the same conditions, which reveals the enhanced photocatalytic activity of the prepared Cu_2O-based heterostructures in the presence of visible light for CO_2 conversion to CH_3OH. Moreover, a similar performance was achieved in our group when using Cu nanoparticles synthesised in ionic liquid and embedded in TiO_2 (Cu/TiO_2) for CO_2-to-CH_3OH photoconversion ($r = 34.4$ μmol·g^{-1}·h^{-1}) [13] with the same operating conditions and experimental setup. It should be noted, however, that the reaction selectivity towards CH_3OH production is superior when employing the $Cu_2O/Mo_2C/TiO_2$ heterostructures developed in this work ($S = 0.93$) with respect to the values achieved at Cu/TiO_2 (*S* ranging from 0.45 to 0.84 as a function of Cu content), displaying also an stable CH_3OH yield after 7 h of operation in contrast to Cu/TiO_2-based surfaces that deactivate with time (please see the supporting information). This may further prove the beneficial synergetic effect between Cu_2O, Mo_2C and TiO_2 in the hererostructures for stable visible ligt-driven CO_2 conversion.

Although there are also studies with improved CH_3OH rates (> 100 μmol·g^{-1}·h^{-1}), it is worth mentioning here the high light intensity applied (e.g., 100 mW·cm^{-2}) in comparison to that of the present study (5 mW·cm^{-2}), which might be partially responsible of such excellent performance. For instance, the application of a light intensity of 100 mW (for 2 h) at Ni@NiO/$InTaO_4$-N photocatalysts led to an improved CH_3OH formation (160 μmol·g^{-1}·h^{-1}) in water media [96]. Similarly, Iqbal and collaborators prepared *p-n-type* $ZnFe_2O_4/TiO_2$ heterojunctions with marked improvements in CH_3OH yield under visible light illumination (100 mW·cm^{-2}; $r = 138.9$ μmol·g^{-1}·h^{-1}) in a KOH/$NaSO_3$/-Na_2S/water-based solvent [102]. Moreover, if we make a comparison between our achievements and those CH_3OH rates reported at Cu_2O--based photoactive materials, similar process performances can be found. For example, a similar formation of CH_3OH per gram of photocatalyst and time ($r = 38.2$ μmol·g^{-1}·h^{-1}) was reached in 2011 at nanocrystallite Cu_2O/SiC materials [90]. The behavior of the developed $Cu_2O/-Mo_2C/TiO_2$ heterostructures is, by contrast, clearly superior than that of Cu_2O/carbon nanoparticles [98], at which a CH_3OH production of 14.1 μmol·g^{-1}·h^{-1} was reported in 2018. The marked improvement might be explained by better visible light absorption properties of the materials in the presence of Mo_2C. Furthermore, the use of carbon quantum dots (CQDs) in Cu_2O/CQDs heterostructures have revealed in 2015 the possibility of improving the material stability and its visible light absorption characteristics, due to the excellent photoinduced electron transfer and optical properties of CQDs, respectively [97]. Thus, the incorporation of CQDs in the photocatalytic structures represents the main reason of an enhanced CH_3OH rate ($r = 55.7$ μmol·g^{-1}·h^{-1}).

Last but not least, it is worth mentioning that all previous systems compared with this work (Fig. 11 and supporting information) do not operate in continuous mode, except for those contributions from our group [13,20]. In other words, the photocatalytic material is usually suspended in the reaction media (slurry batch reactors) and the obtained products must be therefore separated from the photocatalyst, which involves additional process costs and makes the process less suitable for the practical application of the CO_2-to-CH_3OH photocatalytic reaction. This fact consequently denotes the relevance of the present study, where the photocatalyst is deposited onto a porous carbon support (not

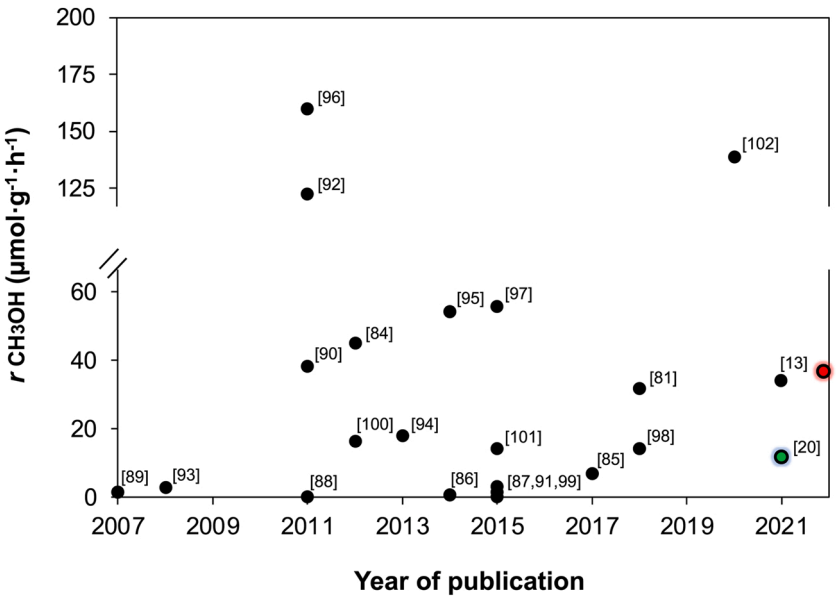

Fig. 11. Comparative analysis on visible light-driven CO_2-to-CH_3OH conversion in aqueous solution in the last years. This work is shown in red and the best result achieved at Cu_2O-free Mo_2C/TiO_2 blends can be seen in green.

suspended in aqueous solution) in a planar optofluidic microreactor that operates in continuous mode for visible light-driven CO_2 conversion to CH_3OH.

4. Conclusions

In this work, we investigate a continuous CO_2 photoreduction to methanol process under visible light in a planar optofluidic microreactor (with more potential for real applications in comparison with conventional batch approaches) using novel $Cu_2O/Mo_2C/TiO_2$ heterostructures. The photoactive surfaces are prepared by airbrushing photocatalytic inks with different Cu_2O loadings over porous carbon paper supports. The characterisation results show that the light-responsive materials present improved optical and absorption properties in the visible region and decreased optical bandgap energies in comparison with bare TiO_2-P25 and Mo_2C/TiO_2 blends, due to the *p-type* semiconductor properties of Cu_2O. Besides, the specific (111) Cu_2O crystal facets found in the prepared heterostructures seem to facilitate CO_2 activation (oxygen-vacancy defects) and electron migration towards an improved selective methanol generation. This leads to an enhanced continuous photoconversion of CO_2 to methanol with Cu4Mo2C4 ($r = 36.3$ μmol•g^{-1}•h^{-1}; $AQY = 0.64\%$; $S = 0.93$) in comparison with the results achieved at Cu_2O-free Mo_2C4 surfaces ($r = 11.8$ μmol•g^{-1}•h^{-1}; $AQY = 0.21\%$; $S = 0.92$). Larger Cu_2O loadings (> 4 wt%), however, seem to hinder the photocatalytic activity of the heterostructures due to particle agglomeration. The system remains stable for methanol production after 7 h of continuous operation in the optofluidic microreactor. The maximum methanol rate achieved in this study outperforms most of the results reported in visible light-driven CO_2-to-methanol photoreduction systems using batch photoreactors (suspended catalysts in aqueous and non-aqueous solvents), explained not only by the microreactor applied but also the efficient heterostructures. Hence, the continuous visible light-driven CO_2 conversion using optofluidic microreactors and $Cu_2O/Mo_2C/TiO_2$ heterostructures constitutes a preferred system from a practical application viewpoint.

CRediT authorship contribution statement

Jonathan Albo, Gonzalo García, Ignacio Hernández: Methodology, Resources, Validation, Supervision, Funding acquisition; **Jonathan Albo, Gonzalo García:** Conceptualization; **Ivan Merino-Garcia, Jonathan Albo, Gonzalo García, Ignacio Hernández:** Formal analysis, Investigation, Writing – original draft, Visualization, Writing – review & editing; **Jonathan Albo:** Project administration.

Declaration of Competing Interest

The authors declare that they have no known competing financial interests or personal relationships that could have appeared to influence the work reported in this paper.

Data Availability

Data will be made available on request.

Acknowledgments

The authors gratefully acknowledge the financial support from Ministerio de Ciencia e Innovación (MCIN) under the projects PID2019-104050RA-I00 and PID2020-117586RB-I00, funded by MCIN/AEI/10.13039/501100011033. G.G. would also like to thank the Canarian Agency for Research, Innovation and Information Society (ACIISI, ProID2021010098), as well as NANOtec, INTech, Cabildo de Tenerife, SEGAI (ULL) for laboratory facilities, and the Laser Spectroscopy and High Pressure Group (ULL) for diffuse reflectance measurements. I.H. also acknowledges the funding by the Spanish Ministry of Economy and Competitiveness, Grant No. MAT2016-80438-P.

Appendix A. Supporting information

Supplementary data associated with this article can be found in the online version at doi:10.1016/j.jcou.2022.102340.

References

[1] R.A. Tufa, D. Chanda, M. Ma, D. Aili, T.B. Demissie, J. Vaes, Q. Li, S. Liu, D. Pant, Towards highly efficient electrochemical CO_2 reduction: cell designs, membranes and electrocatalysts, Appl. Energy 277 (2020), 115557, https://doi.org/10.1016/j.apenergy.2020.115557.

[2] A. Irabien, M. Alvarez-Guerra, J. Albo, A. Dominguez-Ramos, Electrochemical conversion of CO_2 to value-added products, in: Electrochem. Water Wastewater Treat, Elsevier, Amsterdam, 2018, pp. 29–59.

[3] I. Merino-Garcia, J. Albo, P. Krzywda, G. Mul, A. Irabien, Bimetallic Cu-based hollow fibre electrodes for CO_2 electroreduction, Catal. Today 346 (2020) 34–39, https://doi.org/10.1016/j.cattod.2019.03.025.

[4] J. Albo, A. Irabien, Cu_2O-loaded gas diffusion electrodes for the continuous electrochemical reduction of CO_2 to methanol, J. Catal. 343 (2016) 232–239, https://doi.org/10.1016/j.jcat.2015.11.014.

[5] J. Albo, M. Alvarez-Guerra, P. Castaño, A. Irabien, Towards the electrochemical conversion of carbon dioxide into methanol, Green. Chem. 17 (2015) 2304–2324, https://doi.org/10.1039/c4gc02453b.

[6] W. Zhang, Q. Qin, L. Dai, R. Qin, X. Zhao, X. Chen, D. Ou, J. Chen, T.T. Chuong, B. Wu, N. Zheng, Electrochemical reduction of carbon dioxide to methanol on hierarchical Pd/SnO_2 nanosheets with abundant Pd–O–Sn interfaces, in: Chemie-Angew (Ed.), Int, 57, 2018, pp. 9475–9479, https://doi.org/10.1002/anie.201804142.

[7] J. Albo, A. Sáez, J. Solla-Gullón, V. Montiel, A. Irabien, Production of methanol from CO_2 electroreduction at Cu_2O and Cu_2O/ZnO-based electrodes in aqueous solution, Appl. Catal. B Environ. 176–177 (2015) 709–717, https://doi.org/10.1016/j.apcatb.2015.04.055.

[8] S. Castro, J. Albo, A. Irabien, Photoelectrochemical reactors for CO_2 utilization, ACS Sustain. Chem. Eng. 6 (2018) 15877–15894, https://doi.org/10.1021/acssuschemeng.8b03706.

[9] W.A. Thompson, E. Sanchez Fernandez, M.M. Maroto-Valer, Review and analysis of CO_2 photoreduction kinetics, ACS Sustain. Chem. Eng. 8 (2020) 4677–4692, https://doi.org/10.1021/acssuschemeng.9b06170.

[10] Y. Liu, F. Li, X. Zhang, X. Ji, Recent progress on electrochemical reduction of CO_2 to methanol, Curr. Opin. Green. Sustain. Chem. 23 (2020) 10–17, https://doi.org/10.1016/j.cogsc.2020.03.009.

[11] C. Azenha, C. Mateos-Pedrero, M. Alvarez-Guerra, A. Irabien, A. Mendes, Enhancement of the electrochemical reduction of CO_2 to methanol and suppression of H2 evolution over CuO nanowires, Electrochim. Acta 363 (2020), 137207, https://doi.org/10.1016/j.electacta.2020.137207.

[12] S. Payra, S. Shenoy, C. Chakraborty, K. Tarafder, S. Roy, Structure-sensitive electrocatalytic reduction of CO_2 to methanol over carbon-supported intermetallic PtZn nano-alloys, ACS Appl. Mater. Interfaces 12 (2020) 19402–19414, https://doi.org/10.1021/acsami.0c00521.

[13] J. Albo, M.I. Qadir, M. Samperi, J.A. Fernandes, I. de Pedro, J. Dupont, Use of an optofluidic microreactor and Cu nanoparticles synthesized in ionic liquid and embedded in TiO_2 for an efficient photoreduction of CO_2 to methanol, Chem. Eng. J. 404 (2021), 126643, https://doi.org/10.1016/j.cej.2020.126643.

[14] W. Tu, Y. Zhou, Z. Zou, Photocatalytic conversion of CO_2 into renewable hydrocarbon fuels: state-of-the-art accomplishment, challenges, and prospects, Adv. Mater. 26 (2014) 4607–4626, https://doi.org/10.1002/adma.201400087.

[15] J. Albo, M. Alvarez-Guerra, A. Irabien, Electro-, photo-, and photo-electrochemical reduction of CO_2, in: W.Y. Teoh, A. Urakawa, Y.H. Ng, P.H.-L. Sit (Eds.), Heterogeneous Catalysts: Advanced Design, Characterization and Applications, Wiley-VCH GmbH, Weinheim, 2021, https://doi.org/10.1002/9783527813599.ch36.

[16] A. Raza, H. Shen, A.A. Haidry, Novel Cu_2ZnSnS_4/Pt/g-C_3N_4 heterojunction photocatalyst with straddling band configuration for enhanced solar to fuel conversion, Appl. Catal. B Environ. 277 (2020), 119239, https://doi.org/10.1016/j.apcatb.2020.119239.

[17] L. Zhang, L. Zhang, Y. Chen, Y. Zheng, J. Guo, S. Wan, S. Wang, C.K. Ngaw, J. Lin, Y. Wang, CdS/ZnO: a multipronged approach for efficient reduction of carbon dioxide under visible light irradiation, ACS Sustain. Chem. Eng. 8 (2020) 5270–5277, https://doi.org/10.1021/acssuschemeng.0c00190.

[18] Y. Ma, X. Wang, Y. Jia, X. Chen, H. Han, C. Li, Titanium dioxide-based nanomaterials for photocatalytic fuel generations, Chem. Rev. 114 (2014) 9987–10043, https://doi.org/10.1021/cr500008u.

[19] T.P. Nguyen, D.L.T. Nguyen, V.H. Nguyen, T.H. Le, D.V.N. Vo, Q.T. Trinh, S. R. Bae, S.Y. Chae, S.Y. Kim, Q. Van Le, Recent advances in TiO_2-based photocatalysts for reduction of CO_2 to fuels, Nanomaterials 10 (2020) 337, https://doi.org/10.3390/nano10020337.

[20] J. Albo, G. García, Enhanced visible-light photoreduction of CO_2 to methanol over Mo_2C/TiO_2 surfaces in an optofluidic microreactor, React, Chem. Eng. 6 (2021) 304–312, https://doi.org/10.1039/d0re00376j.

[21] F.R. Pomilla, A. Brunetti, G. Marcì, E.I. García-López, E. Fontananova, L. Palmisano, G. Barbieri, CO_2 to liquid fuels: photocatalytic conversion in a continuous membrane reactor, ACS Sustain. Chem. Eng. 6 (2018) 8743–8753, https://doi.org/10.1021/acssuschemeng.8b01073.

[22] J. Dong, Y. Shi, C. Huang, Q. Wu, T. Zeng, W. Yao, A new and stable Mo-Mo_2C modified g-C_3N_4 photocatalyst for efficient visible light photocatalytic H_2 production, Appl. Catal. B Environ. 243 (2019) 27–35, https://doi.org/10.1016/j.apcatb.2018.10.016.

[23] X. Ma, C. Ren, H. Li, X. Liu, X. Li, K. Han, W. Li, Y. Zhan, A. Khan, Z. Chang, C. Sun, H. Zhou, A novel noble-metal-free Mo_2C-In_2S_3 heterojunction photocatalyst with efficient charge separation for enhanced photocatalytic H_2 evolution under visible light, J. Colloid Interface Sci. 582 (2021) 488–495, https://doi.org/10.1016/j.jcis.2020.08.083.

[24] C. Zhang, Y. Zhou, W. Wang, Y. Yang, C. Zhou, L. Wang, L. Lei, D. He, H. Luo, D. Huang, Formation of Mo_2C/hollow tubular g-C_3N_4 hybrids with favorable charge transfer channels for excellent visible-light-photocatalytic performance, Appl. Surf. Sci. 527 (2020), 146757, https://doi.org/10.1016/j.apsusc.2020.146757.

[25] Z. Zhao, G. Lu, Cu-based single-atom catalysts boost electroreduction of CO_2 to CH_3OH: first-principles predictions, J. Phys. Chem. C. 123 (2019) 4380–4387, https://doi.org/10.1021/acs.jpcc.8b12449.

[26] K. Zhao, Y. Liu, X. Quan, S. Chen, H. Yu, C.O.2 electroreduction at low overpotential on oxide-derived Cu/carbons fabricated from metal organic framework, ACS Appl. Mater. Interfaces 9 (2017) 5302–5311, https://doi.org/10.1021/acsami.6b15402.

[27] L. Zhang, I. Merino-Garcia, J. Albo, C.M. Sánchez-Sánchez, Electrochemical CO_2 reduction reaction on cost-effective oxide-derived copper and transition metal–nitrogen–carbon catalysts, Curr. Opin. Electrochem. 23 (2020) 65–73, https://doi.org/10.1016/j.coelec.2020.04.005.

[28] J. Yuan, C. Hao, Solar-driven photoelectrochemical reduction of carbon dioxide to methanol at $CuInS_2$ thin film photocathode, Sol. Energy Mater. Sol. Cells 108 (2013) 170–174, https://doi.org/10.1016/j.solmat.2012.09.024.

[29] L. Anton Wein, H. Zhang, K. Urushidate, M. Miyano, Y. Izumi, Optimized photoreduction of CO_2 exclusively into methanol utilizing liberated reaction space in layered double hydroxides comprising zinc, copper, and gallium, Appl. Surf. Sci. 447 (2018) 687–696, https://doi.org/10.1016/j.apsusc.2018.04.046.

[30] I.H. Tseng, J.C.S. Wu, H.Y. Chou, Effects of sol-gel procedures on the photocatalysis of Cu/TiO_2 in CO_2 photoreduction, J. Catal. 221 (2004) 432–440, https://doi.org/10.1016/j.jcat.2003.09.002.

[31] M. Cheng, S. Yang, R. Chen, X. Zhu, Q. Liao, Y. Huang, Copper-decorated TiO_2 nanorod thin films in optofluidic planar reactors for efficient photocatalytic reduction of CO_2, Int. J. Hydrog. Energy 42 (2017) 9722–9732, https://doi.org/10.1016/j.ijhydene.2017.01.126.

[32] A.D. Handoko, J. Tang, Controllable proton and CO_2 photoreduction over Cu_2O with various morphologies, Int. J. Hydrog. Energy 38 (2013) 13017–13022, https://doi.org/10.1016/j.ijhydene.2013.03.128.

[33] F. Li, L. Zhang, J. Tong, Y. Liu, S. Xu, Y. Cao, S. Cao, Photocatalytic CO_2 conversion to methanol by Cu_2O/graphene/TNA heterostructure catalyst in a visible-light-driven dual-chamber reactor, Nano Energy 27 (2016) 320–329, https://doi.org/10.1016/j.nanoen.2016.06.056.

[34] B. Li, W. Niu, Y. Cheng, J. Gu, P. Ning, Q. Guan, Preparation of Cu_2O modified TiO_2 nanopowder and its application to the visible light photoelectrocatalytic reduction of CO_2 to CH_3OH, Chem. Phys. Lett. 700 (2018) 57–63, https://doi.org/10.1016/j.cplett.2018.03.049.

[35] J. Zhou, Y. Li, L. Yu, Z. Li, D. Xie, Y. Zhao, Y. Yu, Facile in situ fabrication of Cu_2O@Cu metal-semiconductor heterostructured nanorods for efficient visible-light driven CO_2 reduction, Chem. Eng. J. 385 (2020), 123940, https://doi.org/10.1016/j.cej.2019.123940.

[36] S. Kazemi Movahed, A. Najinasab, R. Nikbakht, M. Dabiri, Visible light assisted photocatalytic reduction of CO_2 to methanol using Fe_3O_4@N-C/Cu_2O nanostructure photocatalyst, J. Photochem. Photobiol. A Chem. 401 (2020), 112763, https://doi.org/10.1016/j.jphotochem.2020.112763.

[37] V.H. Nguyen, J.C.S. Wu, Recent developments in the design of photoreactors for solar energy conversion from water splitting and CO_2 reduction, Appl. Catal. A Gen. 550 (2018) 122–141, https://doi.org/10.1016/j.apcata.2017.11.002.

[38] A. Francis, S. Shanmuga Priya, S. Harish Kumar, K. Sudhakar, M. Tahir, A review on recent developments in solar photoreactors for carbon dioxide conversion to fuels, J. CO_2 Util. 47 (2021), 101515, https://doi.org/10.1016/j.jcou.2021.101515.

[39] K. Li, X. An, K.H. Park, M. Khraisheh, J. Tang, A critical review of CO_2 photoconversion: catalysts and reactors, Catal. Today 224 (2014) 3–12, https://doi.org/10.1016/j.cattod.2013.12.006.

[40] X. Cheng, R. Chen, X. Zhu, Q. Liao, X. He, S. Li, L. Li, Optofluidic membrane microreactor for photocatalytic reduction of CO_2, Int. J. Hydrog. Energy 41 (2016) 2457–2465, https://doi.org/10.1016/j.ijhydene.2015.12.066.

[41] X. Cheng, R. Chen, X. Zhu, Q. Liao, L. An, D. Ye, X. He, S. Li, L. Li, An optofluidic planar microreactor for photocatalytic reduction of CO_2 in alkaline environment, Energy 120 (2017) 276–282, https://doi.org/10.1016/j.energy.2016.11.081.

[42] R. Guil-López, E. Nieto, J.A. Botas, J.L.G. Fierro, On the genesis of molybdenum carbide phases during reduction-carburization reactions, J. Solid State Chem. 190 (2012) 285–295, https://doi.org/10.1016/j.jssc.2012.02.021.

[43] W. Kim, T. Seok, W. Choi, Nafion layer-enhanced photosynthetic conversion of CO_2 into hydrocarbons on TiO_2 nanoparticles, Energy Environ. Sci. 5 (2012) 6066–6070, https://doi.org/10.1039/c2ee03338k.

[44] J.Y. Lee, J.H. Choi, Sonochemical synthesis of Ce-doped TiO_2 nanostructure: a visible-light-driven photocatalyst for degradation of toluene and O-Xylene, Mater. (Basel) 12 (2019) 1265, https://doi.org/10.3390/ma12081265.

[45] M.Á. López Zavala, S.A. Lozano Morales, M. Ávila-Santos, Synthesis of stable TiO_2 nanotubes: effect of hydrothermal treatment, acid washing and annealing temperature, Heliyon 3 (2017), e00456, https://doi.org/10.1016/j.heliyon.2017.e00456.

[46] G. García, O. Guillén-Villafuerte, J.L. Rodríguez, M.C. Arévalo, E. Pastor, Electrocatalysis on metal carbide materials, Int. J. Hydrog. Energy 41 (2016) 19664–19673, https://doi.org/10.1016/j.ijhydene.2016.04.146.

[47] A.M. Taddesse, M. Alemu, T. Kebede, Enhanced photocatalytic activity of p-n-n heterojunctions ternary composite Cu_2O/ZnO/Ag_3PO_4 under visible light irradiation, J. Environ. Chem. Eng. 8 (2020), 104356, https://doi.org/10.1016/j.jece.2020.104356.

[48] H. Cheng, J. Wang, Y. Zhao, X. Han, Effect of phase composition, morphology, and specific surface area on the photocatalytic activity of TiO_2 nanomaterials, RSC Adv. 4 (2014) 47031–47038, https://doi.org/10.1039/c4ra05509h.

[49] J. Zhang, P. Zhou, J. Liu, J. Yu, New understanding of the difference of photocatalytic activity among anatase, rutile and brookite TiO_2, Phys. Chem. Chem. Phys. 16 (2014) 20382–20386, https://doi.org/10.1039/c4cp02201g.

[50] B. Liu, X. Yao, Z. Zhang, C. Li, J. Zhang, P. Wang, J. Zhao, Y. Guo, J. Sun, C. Zhao, Synthesis of Cu_2O nanostructures with tunable crystal facets for electrochemical

CO_2 reduction to alcohols, ACS Appl. Mater. Interfaces 13 (2021) 39165–39177, https://doi.org/10.1021/acsami.1c03850.
[51] A. Sahai, N. Goswami, S.D. Kaushik, S. Tripathi, Cu/Cu_2O/CuO nanoparticles: novel synthesis by exploding wire technique and extensive characterization, Appl. Surf. Sci. 390 (2016) 974–983, https://doi.org/10.1016/j.apsusc.2016.09.005.
[52] I. Merino-Garcia, J. Albo, A. Irabien, Productivity and selectivity of gas-phase CO_2 electroreduction to methane at copper nanoparticle-based electrodes, Energy Technol. 5 (2017) 922–928, https://doi.org/10.1002/ente.201600616.
[53] T.Y. Chang, R.M. Liang, P.W. Wu, J.Y. Chen, Y.C. Hsieh, Electrochemical reduction of CO_2 by Cu_2O-catalyzed carbon clothes, Mater. Lett. 63 (2009) 1001–1003, https://doi.org/10.1016/j.matlet.2009.01.067.
[54] E. Andrews, M. Ren, F. Wang, Z. Zhang, P. Sprunger, R. Kurtz, J. Flake, Electrochemical reduction of CO_2 at Cu nanocluster / (1010) ZnO electrodes, J. Electrochem. Soc. 160 (2013) H841–H846, https://doi.org/10.1149/2.105311jes.
[55] M.E. Aguirre, R. Zhou, A.J. Eugene, M.I. Guzman, M.A. Grela, Cu_2O/TiO_2 heterostructures for CO_2 reduction through a direct Z-scheme: protecting Cu_2O from photocorrosion, Appl. Catal. B Environ. 217 (2017) 485–493, https://doi.org/10.1016/j.apcatb.2017.05.058.
[56] S. Kavitha, N. Jayamani, D. Barathi, A study on preparation of unique TiO_2/Cu_2O nanocomposite with highly efficient photocatalytic reactivity under visible-light irradiation, Mater. Technol. 36 (2021) 670–683, https://doi.org/10.1080/10667857.2020.1786785.
[57] H. Wang, H. Rong, D. Wang, X. Li, E. Zhang, X. Wan, B. Bai, M. Xu, J. Liu, J. Liu, W. Chen, J. Zhang, Highly selective photoreduction of CO_2 with suppressing H_2 evolution by plasmonic Au/CdSe–Cu_2O hierarchical nanostructures under visible light, Small 16 (2020) 2000426, https://doi.org/10.1002/smll.202000426.
[58] Y. Nakano, S. Saeki, T. Morikawa, Optical bandgap widening of p-type Cu_2O films by nitrogen doping, Appl. Phys. Lett. 94 (2009), 022111, https://doi.org/10.1063/1.3072804.
[59] A. Chen, H. Long, X. Li, Y. Li, G. Yang, P. Lu, Controlled growth and characteristics of single-phase Cu_2O and CuO films by pulsed laser deposition, Vacuum 83 (2009) 927–930, https://doi.org/10.1016/j.vacuum.2008.10.003.
[60] X. Mathew, N.R. Mathews, P.J. Sebastian, Temperature dependence of the optical transitions in electrodeposited Cu_2O thin films, Sol. Energy Mater. Sol. Cells 70 (2001) 277–286, https://doi.org/10.1016/S0927-0248(01)00068-X.
[61] B. Ma, X. Wang, K. Lin, J. Li, Y. Liu, H. Zhan, W. Liu, A novel ultraefficient non-noble metal composite cocatalyst Mo_2N/Mo_2C/graphene for enhanced photocatalytic H_2 evolution, Int. J. Hydrog. Energy 42 (2017) 18977–18984, https://doi.org/10.1016/j.ijhydene.2017.05.212.
[62] S.P. Adhikari, Z.D. Hood, K.L. More, V.W. Chen, A. Lachgar, A visible-light-active heterojunction with enhanced photocatalytic hydrogen generation, ChemSusChem 9 (2016) 1869–1879, https://doi.org/10.1002/cssc.201600424.
[63] T. Jayaraman, S. Arumugam Raja, A. Priya, M. Jagannathan, M. Ashokkumar, Synthesis of visible-light active V_2O_5/g-C_3N_4 heterojunction as an efficient photocatalytic and photoelectrochemical performance, N. J. Chem. 39 (2015) 1367–1374.
[64] I.M. Sundaram, S. Kalimuthu, P. Gomathi priya, Metal-free heterojunction of graphitic carbon nitride composite with superior and stable visible-light active photocatalysis, Mater. Chem. Phys. 204 (2018) 243–250, https://doi.org/10.1016/j.matchemphys.2017.10.041.
[65] V. Etacheri, M.K. Seery, S.J. Hinder, S.C. Pillai, Highly visible light active $TiO_{2-x}N_x$ heterojunction photocatalysts, Chem. Mater. 22 (2010) 3843–3853, https://doi.org/10.1021/cm903260f.
[66] N. Harukawa, S. Murakami, S. Tamon, S. Ijuin, A. Ohmori, K. Abe, T. Shigenari, Temperature dependence of luminescence lifetime in Cu_2O, J. Lumin 87–89 (2000) 1231–1233, https://doi.org/10.1016/S0022-2313(99)00524-4.
[67] F.J. Knorr, C.C. Mercado, J.L. McHale, Trap-state distributions and carrier transport in pure and mixed-phase TiO_2: influence of contacting solvent and interphasial electron transfer, J. Phys. Chem. C. 112 (2008) 12786–12794, https://doi.org/10.1021/jp8039934.
[68] D.K. Pallotti, L. Passoni, P. Maddalena, F. Di Fonzo, S. Lettieri, Photoluminescence mechanisms in anatase and rutile TiO_2, J. Phys. Chem. C. 121 (2017) 9011–9021, https://doi.org/10.1021/acs.jpcc.7b00321.
[69] C. De Oliveira, D.R. Salahub, H.A. De Abreu, H.A. Duarte, Native defects in α-Mo_2C: Insights from first-principles calculations, J. Phys. Chem. C. 118 (2014) 25517–25524, https://doi.org/10.1021/jp507947b.
[70] H. Liu, J. Zhu, Z. Lai, R. Zhao, D. He, A first-principles study on structural and electronic properties of Mo_2C, Scr. Mater. 60 (2009) 949–952, https://doi.org/10.1016/j.scriptamat.2009.02.010.
[71] H. Zhang, G. Yang, X. Zuo, H. Tang, Q. Yang, G. Li, Computational studies on the structural, electronic and optical properties of graphene-like MXenes (M_2CT_2, M = Ti, Zr, Hf; T = O, F, OH) and their potential applications as visible-light driven photocatalysts, J. Mater. Chem. A 4 (2016) 12913–12920, https://doi.org/10.1039/c6ta04628b.
[72] X.H. Zha, J. Yin, Y. Zhou, Q. Huang, K. Luo, J. Lang, J.S. Francisco, J. He, S. Du, Intrinsic structural, electrical, thermal, and mechanical properties of the promising conductor Mo_2C MXene, J. Phys. Chem. C. 120 (2016) 15082–15088, https://doi.org/10.1021/acs.jpcc.6b04192.
[73] J.F. de Brito, A.A. da Silva, A.J. Cavalheiro, M.V.B. Zanoni, Evaluation of the parameters affecting the photoelectrocatalytic reduction of CO_2 to CH_3OH at Cu/Cu_2O electrode, Int. J. Electrochem. Sci. 9 (2014) 5961–5973.
[74] J. Albo, G. Beobide, P. Castaño, A. Irabien, Methanol electrosynthesis from CO_2 at Cu_2O/ZnO prompted by pyridine-based aqueous solutions, J. CO_2 Util. 18 (2017) 164–172, https://doi.org/10.1016/j.jcou.2017.02.003.
[75] A. Roy, H.S. Jadhav, J. Gil Seo, Cu_2O/CuO electrocatalyst for electrochemical reduction of carbon dioxide to methanol, Electroanalysis 33 (2021) 705–712, https://doi.org/10.1002/elan.202060265.
[76] Y.N. Kavil, Y.A. Shaban, R.K. Al Farawati, M.I. Orif, M. Zobidi, S.U.M. Khan, Photocatalytic conversion of CO_2 into methanol over Cu-C/TiO_2 nanoparticles under UV light and natural sunlight, J. Photochem. Photobiol. A Chem. 347 (2017) 244–253, https://doi.org/10.1016/j.jphotochem.2017.07.046.
[77] Z. jun Wang, H. Song, H. Pang, Y. Ning, T.D. Dao, Z. Wang, H. Chen, Y. Weng, Q. Fu, T. Nagao, Y. Fang, J. Ye, Photo-assisted methanol synthesis via CO_2 reduction under ambient pressure over plasmonic Cu/ZnO catalysts, Appl. Catal. B Environ. 250 (2019) 10–16, https://doi.org/10.1016/j.apcatb.2019.03.003.
[78] T.N.Q. Trang, L.T.N. Tu, T.V. Man, M. Mathesh, N.D. Nam, V.T.H. Thu, A high-efficiency photoelectrochemistry of Cu_2O/TiO_2 nanotubes based composite for hydrogen evolution under sunlight, Compos. Part B Eng. 174 (2019), 106969, https://doi.org/10.1016/j.compositesb.2019.106969.
[79] X. Yue, S. Yi, R. Wang, Z. Zhang, S. Qiu, A novel architecture of dandelion-like Mo_2C/TiO_2 heterojunction photocatalysts towards high-performance photocatalytic hydrogen production from water splitting, J. Mater. Chem. A 5 (2017) 10591–10598, https://doi.org/10.1039/c7ta02655b.
[80] Z. Xi, C. Li, L. Zhang, M. Xing, J. Zhang, Synergistic effect of Cu_2O/TiO_2 heterostructure nanoparticle and its high H_2 evolution activity, Int. J. Hydrog. Energy 39 (2014) 6345–6353, https://doi.org/10.1016/j.ijhydene.2014.01.209.
[81] G. Yisilamu, H. Maimaiti, A. Awati, D. Zhang, F. Sun, B. Xu, Preparation of cuprous oxide nanoparticles coated with aminated cellulose for the photocatalytic reduction of carbon dioxide to methanol, Energy Technol. 6 (2018) 1168–1177, https://doi.org/10.1002/ente.201700689.
[82] J. Hazarika, M.S. Manna, Electrochemical reduction of CO_2 to methanol with synthesized Cu_2O nanocatalyst: study of the selectivity, Electrochim. Acta 328 (2019), 135053, https://doi.org/10.1016/j.electacta.2019.135053.
[83] L. Qi, S. Liu, W. Gao, Q. Jiang, Mechanistic understanding of CO_2 electroreduction on Cu_2O, J. Phys. Chem. C. 122 (2018) 5472–5480, https://doi.org/10.1021/acs.jpcc.7b11842.
[84] X. Li, H. Liu, D. Luo, J. Li, Y. Huang, H. Li, Y. Fang, Y. Xu, L. Zhu, Adsorption of CO_2 on heterostructure $CdS(Bi_2S_3)/TiO_2$ nanotube photocatalysts and their photocatalytic activities in the reduction of CO_2 to methanol under visible light irradiation, Chem. Eng. J. 180 (2012) 151–158, https://doi.org/10.1016/j.cej.2011.11.029.
[85] Y. Su, Z. Zhang, H. Liu, Y. Wang, $Cd_{0.2}Zn_{0.8}S$@UiO-66-NH_2 nanocomposites as efficient and stable visible-light-driven photocatalyst for H_2 evolution and CO_2 reduction, Appl. Catal. B Environ. 200 (2017) 448–457, https://doi.org/10.1016/j.apcatb.2016.07.032.
[86] E.S. Baeissa, Green synthesis of methanol by photocatalytic reduction of CO_2 under visible light using a graphene and tourmaline co-doped titania nanocomposites, Ceram. Int. 40 (2014) 12431–12438, https://doi.org/10.1016/j.ceramint.2014.04.094.
[87] S. Kawamura, M.C. Puscasu, Y. Yoshida, Y. Izumi, G. Carja, Tailoring assemblies of plasmonic silver/gold and zinc-gallium layered double hydroxides for photocatalytic conversion of carbon dioxide using UV–visible light, Appl. Catal. A Gen. 504 (2015) 238–247, https://doi.org/10.1016/j.apcata.2014.12.042.
[88] N. Ahmed, Y. Shibata, T. Taniguchi, Y. Izumi, Photocatalytic conversion of carbon dioxide into methanol using zinc-copper-M(III) (M = aluminum, gallium) layered double hydroxides, J. Catal. 279 (2011) 123–135, https://doi.org/10.1016/j.jcat.2011.01.004.
[89] P.W. Pan, Y.W. Chen, Photocatalytic reduction of carbon dioxide on NiO/$InTaO_4$ under visible light irradiation, Catal. Commun. 8 (2007) 1546–1549, https://doi.org/10.1016/j.catcom.2007.01.006.
[90] H. Li, Y. Lei, Y. Huang, Y. Fang, Y. Xu, L. Zhu, X. Li, Photocatalytic reduction of carbon dioxide to methanol by Cu_2O/SiC nanocrystallite under visible light irradiation, J. Nat. Gas. Chem. 20 (2011) 145–150, https://doi.org/10.1016/S1003-9953(10)60166-1.
[91] D.S. Lee, Y.W. Chen, Photocatalytic reduction of carbon dioxide with water on $InVO_4$ with NiO cocatalysts, J. CO_2 Util. 10 (2015) 1–6, https://doi.org/10.1016/j.jcou.2015.02.005.
[92] X. Li, J. Chen, H. Li, J. Li, Y. Xu, Y. Liu, J. Zhou, Photoreduction of CO_2 to methanol over Bi_2S_3/CdS photocatalyst under visible light irradiation, J. Nat. Gas. Chem. 20 (2011) 413–417, https://doi.org/10.1016/S1003-9953(10)60212-5.
[93] H.C. Chen, H.C. Chou, J.C.S. Wu, H.Y. Lin, Sol-gel prepared $InTaO_4$ and its photocatalytic characteristics, J. Mater. Res 23 (2008) 1364–1370, https://doi.org/10.1557/jmr.2008.0172.
[94] M. Abou Asi, L. Zhu, C. He, V.K. Sharma, D. Shu, S. Li, J. Yang, Y. Xiong, Visible-light-harvesting reduction of CO_2 to chemical fuels with plasmonic Ag@AgBr/CNT nanocomposites, Catal. Today 216 (2013) 268–275, https://doi.org/10.1016/j.cattod.2013.05.021.
[95] C. Tang, W. Hou, E. Liu, X. Hu, J. Fan, CeF_3/TiO_2 composite as a novel visible-light-driven photocatalyst based on upconversion emission and its application for photocatalytic reduction of CO_2, J. Lumin 154 (2014) 305–309, https://doi.org/10.1016/j.jlumin.2014.04.040.
[96] C. Tsai, H.M. Chen, R. Liu, K. Asakura, T. Chan, Ni@NiO Core-Shell Structure-Modified Nitrogen-Doped InTaO4 for Solar-Driven Highly Efficient CO2 Reduction to Methanol, 115 (2011) 10180–10186.
[97] H. Li, X. Zhang, D.R. MacFarlane, Carbon quantum dots/Cu_2O heterostructures for solar-light-driven conversion of CO_2 to methanol, Adv. Energy Mater. 5 (2015) 1–6, https://doi.org/10.1002/aenm.201401077.
[98] Z. Dedong, H. Maimaiti, A. Awati, G. Yisilamu, S. Fengchang, W. Ming, Synthesis and photocatalytic CO_2 reduction performance of Cu_2O/Coal-based carbon

nanoparticle composites, Chem. Phys. Lett. 700 (2018) 27–35, https://doi.org/10.1016/j.cplett.2018.04.007.
[99] H. Abdullah, M.R. Khan, M. Pudukudy, Z. Yaakob, N.A. Ismail, CeO_2-TiO_2 as a visible light active catalyst for the photoreduction of CO_2 to methanol, J. Rare Earths 33 (2015) 1155–1161, https://doi.org/10.1016/S1002-0721(14)60540-8.
[100] H. Cheng, B. Huang, Y. Liu, Z. Wang, X. Qin, X. Zhang, Y. Dai, An anion exchange approach to Bi_2WO_6 hollow microspheres with efficient visible light photocatalytic reduction of CO_2 to methanol, Chem. Commun. 48 (2012) 9729–9731, https://doi.org/10.1039/c2cc35289c.
[101] W. Dai, H. Xu, J. Yu, X. Hu, X. Luo, X. Tu, L. Yang, Photocatalytic reduction of CO_2 into methanol and ethanol over conducting polymers modified Bi_2WO_6 microspheres under visible light, Appl. Surf. Sci. 356 (2015) 173–180, https://doi.org/10.1016/j.apsusc.2015.08.059.
[102] F. Iqbal, A. Mumtaz, S. Shahabuddin, M.I. Abd Mutalib, M.S. Shaharun, T. D. Nguyen, M.R. Khan, B. Abdullah, Photocatalytic reduction of CO_2 to methanol over $ZnFe_2O_4$/TiO_2 (p–n) heterojunctions under visible light irradiation, J. Chem. Technol. Biotechnol. 95 (2020) 2208–2221, https://doi.org/10.1002/jctb.6408.
[103] P. Kumar, C. Joshi, A. Barras, B. Sieber, A. Addad, L. Boussekey, S. Szunerits, R. Boukherroub, S.L. Jain, Core–shell structured reduced graphene oxide wrapped magnetically separable rGO@CuZnO@Fe_3O_4 microspheres as superior photocatalyst for CO_2 reduction under visible light, Appl. Catal. B Environ. 205 (2017) 654–665, https://doi.org/10.1016/j.apcatb.2016.11.060.
[104] P. Kumar, B. Sain, S.L. Jain, Photocatalytic reduction of carbon dioxide to methanol using a ruthenium trinuclear polyazine complex immobilized on graphene oxide under visible light irradiation, J. Mater. Chem. A 2 (2014) 11246–11253, https://doi.org/10.1039/c4ta01494d.
[105] S. Kumari, R. Gusain, A. Kumar, N. Manwar, S.L. Jain, O.P. Khatri, Direct growth of nanostructural MoS_2 over the h-BN nanoplatelets: An efficient heterostructure for visible light photoreduction of CO_2 to methanol, J. CO_2 Util. 42 (2020), 101345, https://doi.org/10.1016/j.jcou.2020.101345.
[106] A. Kumar, P. Kumar, R. Borkar, A. Bansiwal, N. Labhsetwar, S.L. Jain, Metal-organic hybrid: Photoreduction of CO_2 using graphitic carbon nitride supported heteroleptic iridium complex under visible light irradiation, Carbon 123 (2017) 371–379, https://doi.org/10.1016/j.carbon.2017.07.080.
[107] P. Kumar, S. Kumar, S. Cordier, S. Paofai, R. Boukherroub, S.L. Jain, Photoreduction of CO_2 to methanol with hexanuclear molybdenum $[Mo_6Br_{14}]^{2-}$ cluster units under visible light irradiation, RSC Adv. 4 (2014) 10420–10423, https://doi.org/10.1039/C3RA47255H.
[108] P. Kumar, H.P. Mungse, O.P. Khatri, S.L. Jain, Nitrogen-doped graphene-supported copper complex: a novel photocatalyst for CO_2 reduction under visible light irradiation, RSC Adv. 5 (2015) 54929–54935, https://doi.org/10.1039/c5ra05319f.
[109] R. Gusain, P. Kumar, O.P. Sharma, S.L. Jain, O.P. Khatri, Reduced graphene oxide-CuO nanocomposites for photocatalytic conversion of CO_2 into methanol under visible light irradiation, Appl. Catal. B Environ. 181 (2016) 352–362, https://doi.org/10.1016/j.apcatb.2015.08.012.
[110] P. Kumar, C. Joshi, N. Labhsetwar, R. Boukherroub, S.L. Jain, A novel Ru/TiO_2 hybrid nanocomposite catalyzed photoreduction of CO_2 to methanol under visible light, Nanoscale 7 (2015) 15258–15267, https://doi.org/10.1039/C5NR03712C.
[111] N. Singhal, R. Goyal, U. Kumar, Visible-light-assisted photocatalytic CO_2 reduction over $InTaO_4$: selective methanol formation, Energy Fuels 31 (2017) 12434–12438, https://doi.org/10.1021/acs.energyfuels.7b02123.
[112] J.O. Olowoyo, M. Kumar, T. Dash, S. Saran, S. Bhandari, U. Kumar, Self-organized copper impregnation and doping in TiO_2 with enhanced photocatalytic conversion of H_2O and CO_2 to fuel, Int. J. Hydrog. Energy 43 (2018) 19468–19480, https://doi.org/10.1016/j.ijhydene.2018.08.209.
[113] A. Kumar, P.K. Prajapati, M.S. Aathira, A. Bansiwal, R. Boukherroub, S.L. Jain, Highly improved photoreduction of carbon dioxide to methanol using cobalt phthalocyanine grafted to graphitic carbon nitride as photocatalyst under visible light irradiation, J. Colloid Interface Sci. 543 (2019) 201–213, https://doi.org/10.1016/j.jcis.2019.02.061.
[114] Q. Mou, Z. Guo, Y. Chai, B. Liu, C. Liu, Visible light assisted production of methanol from CO_2 using CdS@CeO_2 heterojunction, J. Photochem. Photobiol. B Biol. 219 (2021), 112205, https://doi.org/10.1016/j.jphotobiol.2021.112205.
[115] P. Kumar, H.P. Mungse, S. Cordier, R. Boukherroub, O.P. Khatri, S.L. Jain, Hexamolybdenum clusters supported on graphene oxide: visible-light induced photocatalytic reduction of carbon dioxide into methanol, Carbon N. Y 94 (2015) 91–100, https://doi.org/10.1016/j.carbon.2015.06.029.
[116] P.K. Prajapati, S.L. Jain, Synthesis and evaluation of CoPc grafted bismuth oxyhalide ($Bi_{24}O_{31}Br_{10}$): a visible light-active photocatalyst for CO_2 reduction into methanol, Dalt. Trans. 48 (2019) 4941–4948, https://doi.org/10.1039/c9dt00792j.